Digitally Assisted Harmonic Cancellation for Multi-Octave Filter-Less Transmitter

HEMANT KUMAR SINGHAL [1,2], **(Member, IEEE),**
AND KARUN RAWAT [1], **(Senior Member, IEEE)**

[1]Department of Electronics and Communication Engineering, Indian Institute of Technology Roorkee, Roorkee 247667, India
[2]National Institute of Technology, Uttarakhand, Srinagar 246174, India

Corresponding author: Karun Rawat (karunrawat@gmail.com)

ABSTRACT This paper presents and demonstrates the design of a filter-less transmitter architecture with digitally assisted harmonic cancellation. A neural network is used to model the harmonics as well as IMD for digital predistortion applications. This neural network-based harmonic modeling does not require any reference signal to be injected at the input of PA, thereby reducing the complexity in characterizing the harmonics. An in-house 10 W PA operating from VHF to L-band has been designed and characterized for its harmonic suppression. This PA is used along with agile RF transceiver AD9361 from Analog Device and Xilinx embedding platform using Zynq ZC-706 system-on-chip for implementing the entire transmitter. The receiver of AD9361 captures the nonlinearity of the PA in terms of harmonics as well as intermodulation distortion (IMD) components for modeling and predistortion. The proposed architecture can handle all types of distortions due to hardware as well as PA nonlinearity. Besides, it is also able to cancel the harmonics using a harmonic injection in the feed-forward configuration. This transmitter architecture has the advantages of being low cost, filter-less, wideband, frequency agile, reconfigurable and less bulky compared to the conventional scheme. The proposed scheme is demonstrated to transmit 5 MHz LTE signal at different frequencies over the range of 100 MHz to 400 MHz. In such a case, the second and third harmonics appear over the frequency range from 200 MHz to 1.2 GHz, which are within the amplification range of PA, yet they are suppressed without using any filter at the output. More than −40 dBc harmonic rejection is achieved over the entire operating range of this filter-less transmitter. The adjacent channel leakage ratio (ACLR) is always better than −45 dBc after applying digital predistortion.

INDEX TERMS Power amplifier, software-defined radio, filter-less, harmonic injection, neural network, non-linear characterization, digital predistortion, feed-forward cancellation.

I. INTRODUCTION

The rapid evolution of wireless standards demands a radio platform that is transparent to all the existing standards. Since these standards may not operate with the same frequency spectrum and modulation schemes, a multi-standard/multi-mode software-defined radio (SDR) is considered as one viable solution [1]. The radio functionalities of SDR can be rapidly configured to any standard with software control. The radio frequency (RF) transmitter in such SDR must operate over a wide range of radio spectrum for backward compatibility. This enables the handling of existing as well as upcoming

wireless standards simultaneously. Moreover, it can also provide backward compatibility to the old generation of wireless communication. Therefore, the upcoming RF transmitter architecture must offer wide bandwidth with operating range, even extending to multi-octave frequencies. In addition, the tactical radios operating in VHF/UHF band also require multi-octave RF transmitters [2]–[5]. The key problem in such multi-octave transmitters is to handle harmonics generated within the band of operation. These harmonics are generated due to the non-linear power amplifier (PA). One conventional way is to operate PA well below from its saturation in the linear region, but this results in poor DC to RF conversion efficiency. This poor efficiency not only results in wastage of energy but also requires costly as well as a bulky

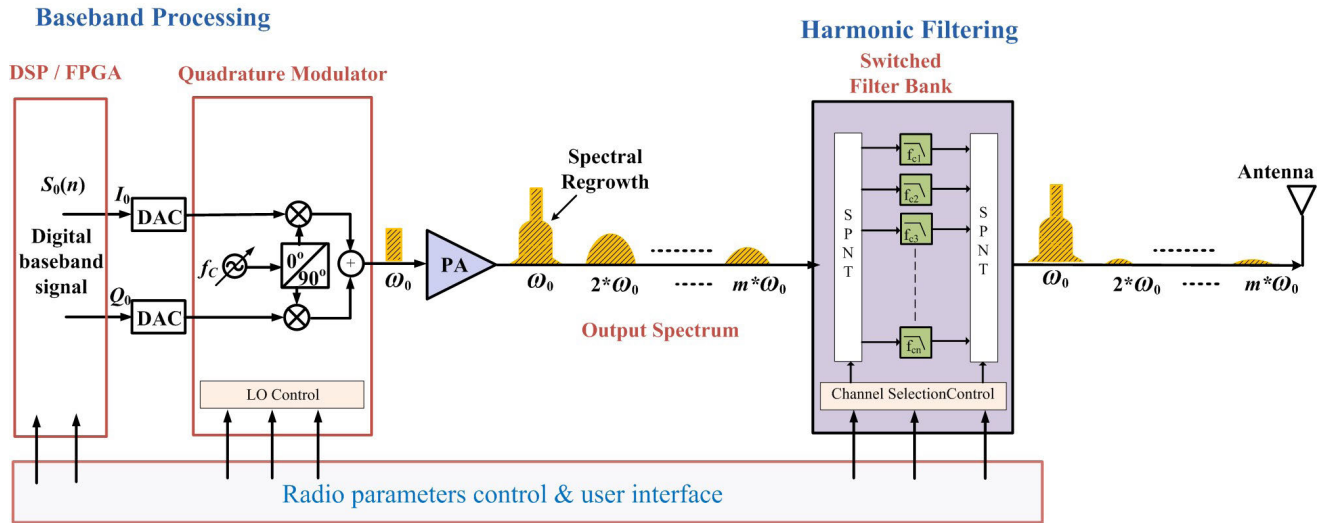The associate editor coordinating the review of this manuscript and approving it for publication was Rocco Giofrè.

Baseband Processing

Harmonic Filtering

FIGURE 1. Conventional multi-octave transmitter.

mechanism for heat dissipation and cooling to ensure reliable operation. Nevertheless, merely operating PA in the back-off region may not fulfill the harmonic suppression requirements for several applications. In the case of multi-octave PAs, any harmonic falling within the operating range will be amplified and, therefore, must be removed before transmission. Using an RF filter can suppress these harmonics. However, a multi-octave transmitter requires switched filter bank to select an operating band/channel while rejecting its harmonics. Fig. 1 shows a typical architecture of SDR with multi-octave operating range using a switched filter bank to select a channel at any instance of time. One can see that the baseband signal is generated digitally, which can be reconfigured to handle any modulation scheme. A radio parameter control unit with user interface can help in digitally configuring such radio, as shown in Fig. 1. This can be a microcontroller or an Advanced RISC Machines (ARM) processor, depending on the functions that have to be carried out in SDR. One can see in Fig. 1 that the local oscillator (LO) of quadrature modulator (QMD) is also reconfigurable with digital control. This can upconvert the baseband signal to any carrier frequency over the multi-octave band. The PA can operate over the multi-octave frequency range and can amplify any signal fed over this range by QMD. Once setting the carrier frequency ω_0 by the LO of QMD, the switched filter bank is also configured to the same operating frequency to create a pass-band at ω_0, while other frequencies especially harmonics $2\omega_0, 3\omega_0 \cdots m\omega_0$ are rejected due to stop-band of the filter. Here, m is an integer representing the order of the harmonic. One can see from Fig. 1 that to handle n-channels, single-pole n-throw (SPNT) switches can be used, which are bulky as well as costly, especially when the multi-octave transmitter is covering UHF/VHF range. Fig. 1 also shows that the spectrum of harmonics is spread and is not similar to the spectrum of the signal at the fundamental frequency.

Moreover, the spectral leakage is also present near the band at ω_0 due to PA nonlinearity. Since the spectral leakage is very close to the signal band, the filter cannot suppress it. Thus, linearization technique such as digital predistortion (DPD) is employed to suppress this spectral regrowth around the desired signal before the transmission [6]–[8]. DPD is one common scheme for linearization, where the nonlinear behavior in terms of intermodulation distortion (or spectral regrowth near the band) is captured and modeled to generate an inverse model of the PA. The baseband signal, when processed through this inverse model, can predistort the signal in such a manner that when it passes through, the PA will compensate for the non-linear distortions generated by the PA. Since DPD requires capturing the non-linear behavior of PA generating IMD, one can also think of capturing and modeling the non-linear behavior of PA generating harmonics. This non-linear model can imitate the behavior of PA and generate the exact harmonic content of PA digitally, which can later be used to cancel the harmonics at the PA output. This digitally controlled harmonic cancellation techniques can omit the switched filter bank, as shown in Fig. 1, and result into filter-less multi-octave transmitter architecture [9]–[15]. This filter-less multi-octave transmitter architecture can present frequency agile and miniaturized solution in VHF/UHF bands particularly suitable for SDR application. The harmonic modeling in [9]–[11] requires additional reference signals to be injected at the input of the PA. Therefore, to employ these models in feed-forward cancellation requires the signals injection at both the input and output at harmonic frequencies. This results in more complex and bulky architecture as the number of harmonics increases. Besides, this may add to power consumption in the case of high power transmitters. Therefore, most of these works are validated up to 2nd harmonic cancellation. The models reported in [12]–[15] claims that they do not require

the injection of the reference signals at the input of PA for harmonic modeling. This is because of their special and rare scenario where the concurrent multi-band transmission happens at harmonically related frequencies. In such a case, the signals transmitted in second and third band coincide with the 2nd and 3rd harmonics of the signal transmitted in the first band acting as reference signals for the harmonic modeling.

This paper presents a new filter-less transmitter architecture capable of compensating 2nd and 3rd harmonics generated by PA using a digitally assisted feed-forward harmonic cancellation scheme. The key contribution of this work is the modeling of harmonics using a real-valued focused time-delay neural network (RVFTDNN), which does not require any reference signal at the input of the PA for harmonic modeling. Thus, it can also be used in any generic case of concurrent multi-band transmission without any specific relation between the concurrent transmission bands. The harmonic models are independently optimized in terms of the number of layers and the number of neurons in each layer. Moreover, an appropriate optimization algorithm has been chosen for fast convergence. These harmonic models are then used to generate harmonics in auxiliary paths which are combined at the PA output for feed-forward harmonic cancellation scheme.

The proposed scheme is validated using a commercial DSP/FPGA board and agile RF transceiver AD9361 from Analog device. Since this board has a limitation in terms of DAC bandwidth as well as independent tuning of LOs; the 2nd and 3rd harmonics are canceled one by one. Later, the simultaneous cancellation of 2nd and 3rd harmonics using wideband DACs and one auxiliary path is validated with instrument-based test-bed. To compensate for IMD, DPD is also performed for linearization. It is worth mentioning that although DPD and PA design at VHF are well-established techniques, they are also discussed for completing the overall filter-less transmitter implementation. Therefore, this work implements and validates new filter-less transmitter architecture capable of compensating all types of distortions, including IMD, as well as harmonics. The scheme is implemented to validate it as simpler solution than other feed-forward harmonic cancellation architecture handling multiple harmonics over the multi-octave operating range. The experimental validation also benchmarks the new filter-less transmitter architecture against the conventional architecture using switched filter bank.

This paper is organized as follows. Section II describes the proposed design architecture for filter-less transmitter design. Later, the design, simulation, and measurement results of the wideband PA are discussed in Section III. The measurement set-up has been proposed in section IV. This includes capturing the fundamental and harmonic components of the PA output. This section also describes the methodology for a digitally supported feedforward technique for harmonic cancellation and behavioral modeling. The proposed architecture is benchmarked with the state of the art in section V. Section VI

reports the measurement results of PA with proposed filter-less transmitter architecture followed by a conclusion in Section VII.

II. FILTER-LESS TRANSMITTER ARCHITECTURE
The filter-less transmitter must embrace two digital techniques i.e. canceling the harmonics generated and linearization for mitigating IMD terms. The DPD technique for linearization can easily be implemented using signal processing in the baseband unit. However, a feed-forward harmonic cancellation requires a multi-channel transmitter to inject the modeled harmonic content at the output of PA for feed-forward cancellation. These techniques are discussed in the following sections.

A. FEED-FORWARD HARMONIC CANCELLATION
The feedforward harmonic cancellation requires the harmonic generation and injection path in the transmitter. Fig. 2 shows the architecture of the wideband multi-octave filter-less transmitter. One can see that this architecture has an auxiliary channel which injects the digitally generated harmonics after PA. Since these harmonics are generated digitally, an appropriate phase and amplitude can be assigned to them in the baseband. An error amplifier (EA) will amplify the generated harmonics to an appropriate power level such that they can cancel the harmonics generated due to the PA at its output. In many cases, one auxiliary channel can handle multiple harmonics, as shown in Fig. 2, due to the large bandwidth availability in the upcoming digital to analog converter (DAC) technology. In such a case, one wideband combiner is sufficient to inject the amplified harmonics after EA in the main PA output for feed-forward cancellation. However, if the DACs have limited bandwidth, the number of auxiliary paths may have to be increased to generate harmonics independently. In such a case, these harmonics can be combined before EA, and still, one wideband combiner is needed after PA. This will save the power loss at the output of PA. Also, in many cases, the requirement of harmonic cancellation is up to 3rd harmonic only, where such configuration presents an excellent alternative to the bulky conventional transmitter with the switched filter bank. A digital feed-forward cancellation of harmonics depends on the following two factors: (a) accuracy of the harmonic model (b) channel distortion and delay presented to the injected harmonic signals in the auxiliary channel. The accuracy of the harmonic model can be increased by using an effective modeling tool such as a neural network (NN). To compensate for the channel distortion and time delay in the auxiliary channel, the harmonic signals to be injected must be generated using the accurate harmonic model. A detailed analysis of the signal modeling, including capturing the signal and time alignment is described in section IV.

B. DIGITAL PREDISTORTION FOR IMD CANCELLATION
In order to cancel out the IMDs generated by PA, a DPD is used to improve adjacent channel suppression near the
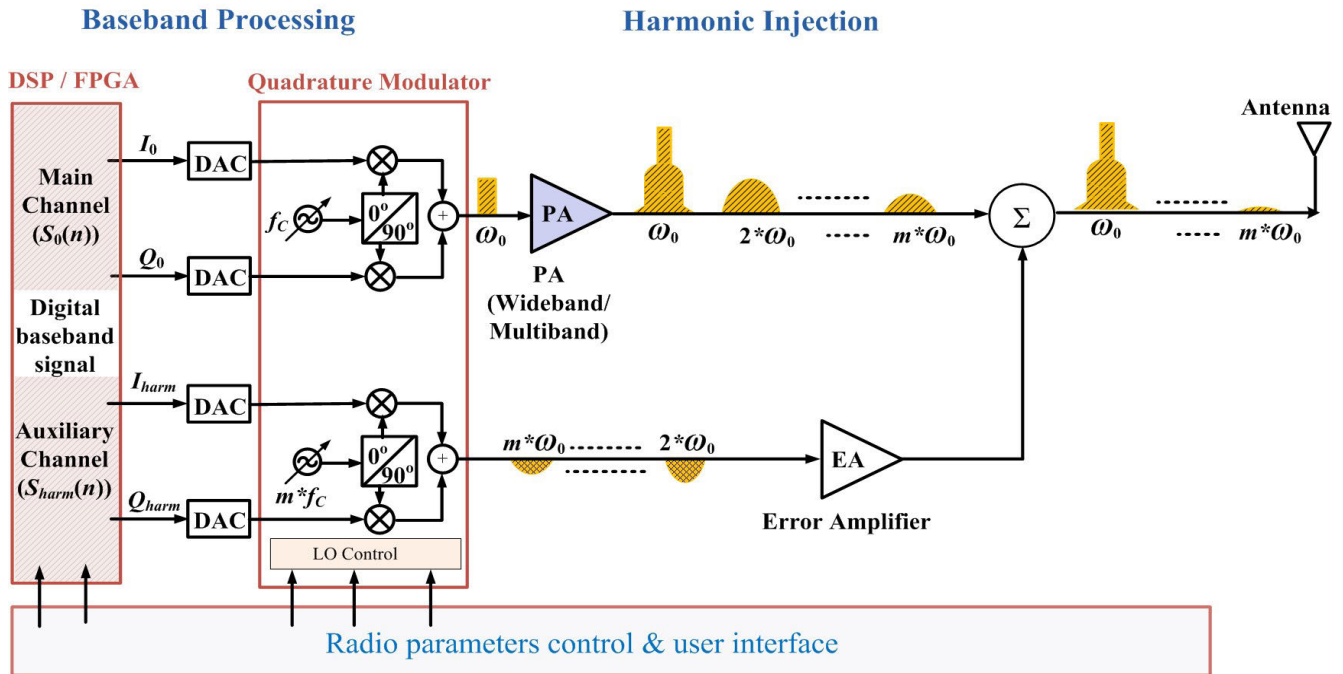
FIGURE 2. Feedforward topology for digital harmonic cancellation in multi-octave filter-less transmitter architecture.
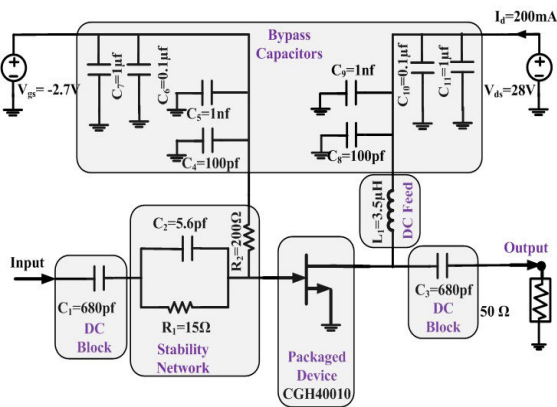

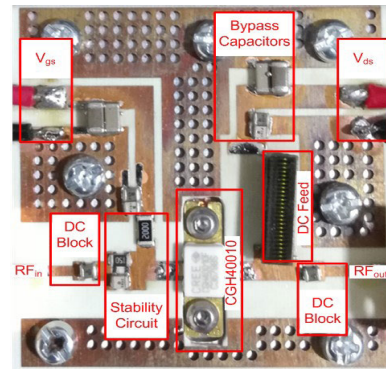**FIGURE 3.** Schematic of 10-watt power amplifier.

FIGURE 4. Photograph of PA prototype with 10 W GaN HEMT device.

fundamental signal. First, the IMD components generated due to the nonlinearity in PA are captured. Second, the PA nonlinearity generating these components are modeled using the captured data. Third, an inverse model is then trained, which is used to predistort the baseband signal before sending it to the DACs in the main channel. The predistorted signal at the fundamental frequency is upconverted to the selected operating frequency using a QMD in the main path. This signal, when passed through PA, will compensate for the IMD components resulting into the linearized and amplified version of the original signal. The parameters of the predistorter are calculated by indirect learning architecture. In this paper, a NN algorithm is also used for the predistorter modeling, which is discussed in section IV.

III. WIDEBAND MULTI-OCTAVE POWER AMPLIFIER DESIGN

The primary objective of the PA design is to achieve broadband operation with output power around 10 W. Therefore, a 10 W Cree device (model number CGH40010) is used for this purpose [16]. Fig. 3 shows the schematic of the PA circuit designed. The device is biased in class AB mode. The device is made unconditionally stable by using using a parallel RC (resistor and capacitor) circuit with R_1 and C_2 and a resistor R_2 in the input, as shown in Fig. 3. After biasing and stabilization, the optimum load can be predicted as $R_{opt} = (V_{dd}-V_k)^2/2P_{out}$, where V_{dd} is the drain bias, V_k is the knee voltage, and P_{out} is the output power. However, the input is conjugate matched. Fig. 4 shows the photograph of the PA design fabricated on microstrip based printed circuit technology. The circuit is printed on a 20 mil thick Rogers
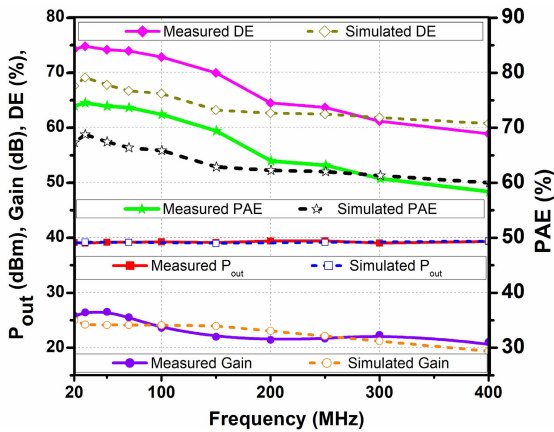
FIGURE 5. Measured and Simulation results of PA prototype over the frequency range.

FIGURE 6. Variation in magnitude of harmonic suppression with respect to fundamental Vs. frequency.

RO4350B dielectric laminate with permittivity $\varepsilon_r = 3.66$ and loss tangent of 0.0031. The PA is tested with continuous wave (CW) signal generated from a signal generator and measuring the output power from the spectrum analyzer. Fig. 5 shows the output power, gain, power added efficiency (PAE), and drain efficiency (DE) measured over a frequency range of 20MHz to 400 MHz. This figure also shows the corresponding simulated results for comparison. Fig 5 shows that the simulated output power is 39.2±0.2 dBm, with 61-69% DE and 60-68.7% PAE over the frequency range from 20 MHz to 400 MHz. The corresponding measured output power, and DE is around 39.2±0.2 dBm and greater than 59% respectively over this frequency range. The 58-74% PAE is achieved in the frequency range. The gain measured at saturation is 23.5 with ±2.5 dB variation over the entire frequency range.

Fig. 6 shows the simulated and measured harmonic distortions over the fundamental frequency range of the PA. One can see that the 2nd and 3rd harmonic suppression is around −15dBc and −20 dBc, respectively in simulation. The measurement results show the minimum suppression of 2nd and 3rd harmonics power as −13 dBc and −18 dBc, respectively over the entire frequency range.

Fig. 7 shows the carrier to 3rd order intermodulation distortion suppression (C/IMD3) for various frequencies within the operating range. The figure shows the C/IMD3 for IMD components at both lower and upper frequencies. These are represented as C/IMD3_L and C/IMD3_U respectively, in Fig. 7. The two tones with frequency spacing of 10MHz are used to obtain this IMD3 response. One can see that near saturation (0-dB back-off), both the C/IMD3_L and C/IMD3_U are nearly same around −15 dBc for various frequencies over the frequency range. It reaches at −30 dBc at 10-12 dB backoff. Later the adjacent channel leakage ratio (ACLR) of the PA is also measured with modulated LTE signals and discussed in section VI. The DPD will also be used to linearize and improve the ACLR in section VI.
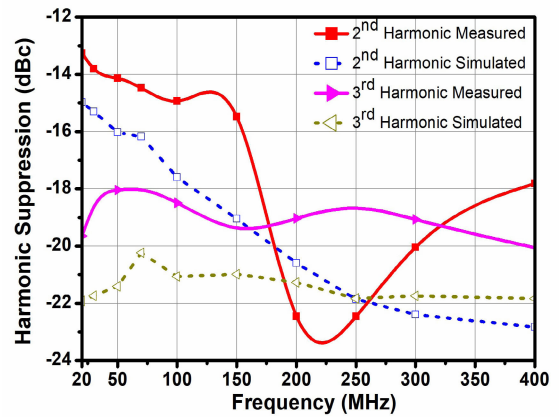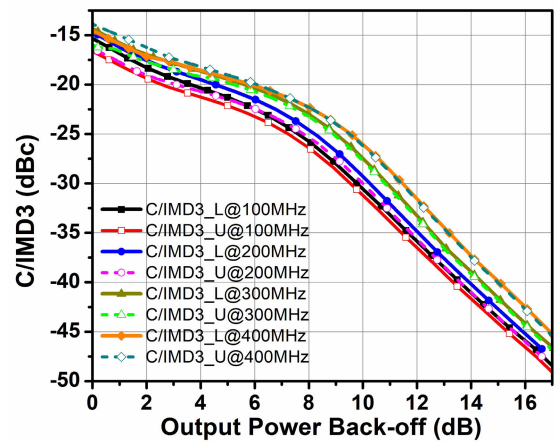

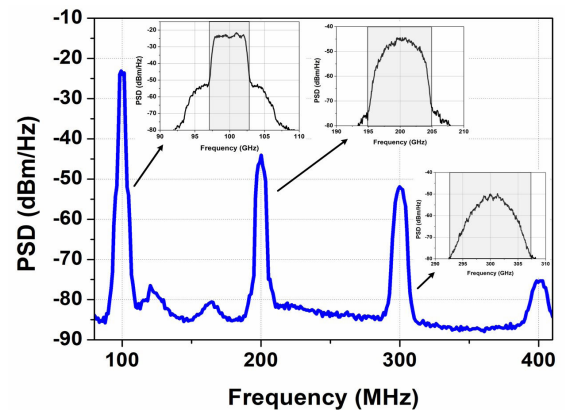**FIGURE 7.** Measured C/IMD3 results over the frequency band.

FIGURE 8. The output spectrum of input 5 MHz LTE signal.

IV. FILTER-LESS TRANSMITTER DESIGN

After CW measurement, the PA is driven with a 5 MHz long term evolution (LTE) signal. The LTE signal being used here has a peak-to-average power ratio (PAPR) of 9.5 dB. The output spectrum of the PA at 100 MHz is shown in Fig. 8.
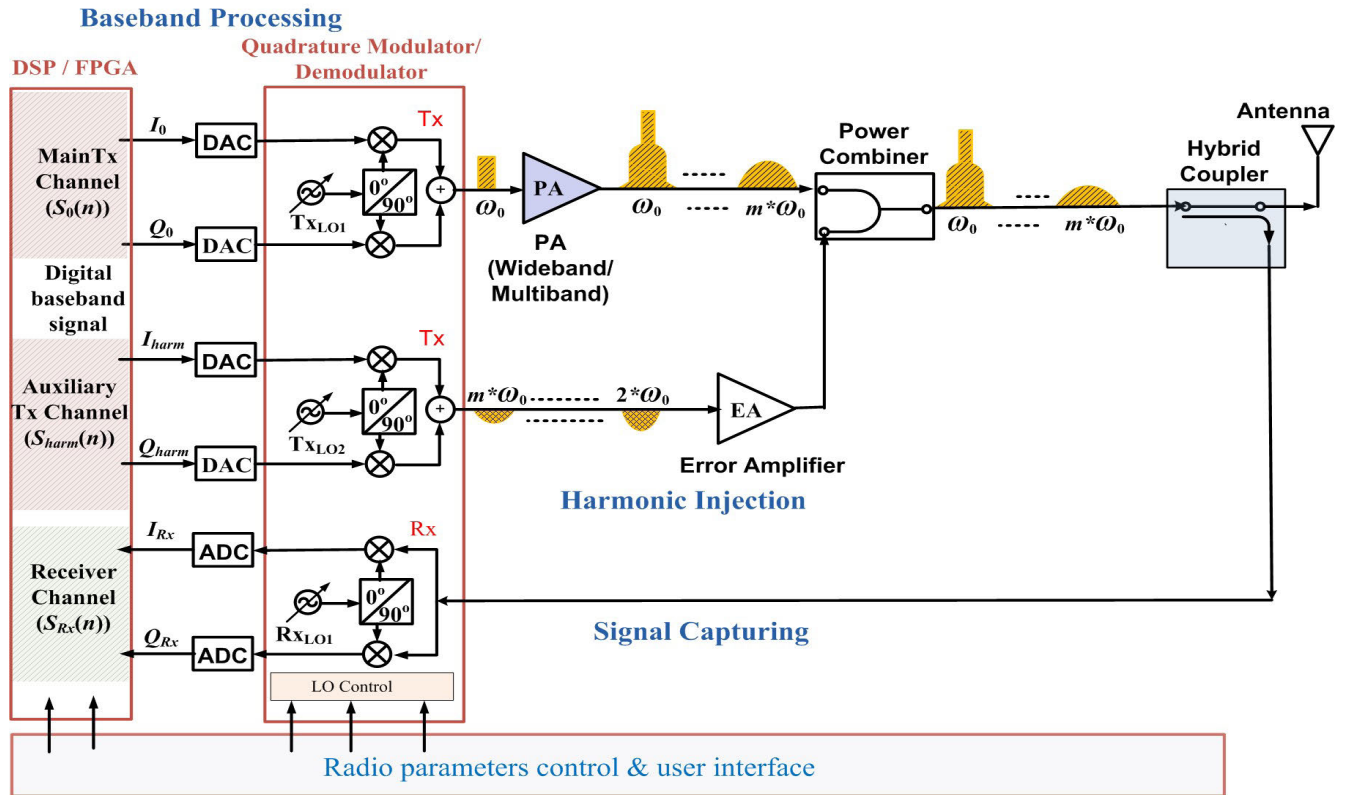
FIGURE 9. Full Setup of distortion-free, harmonic less digitally assisted power amplifier.

One can observe from Fig. 8 that the magnitude of 2nd and 3rd harmonics are more significant than the rest of the harmonics. Also, the bandwidth of 2nd and 3rd harmonics are two and three times, respectively, of that of the fundamental component. The same behavior is also observed for the rest of the frequencies over the band. Hence, the authors have mainly focused on canceling the 2nd and 3rd harmonics of the PA. However, it is worth mentioning that other harmonics can also be canceled in a similar manner if required. One can see from Fig. 8 that there is spectral regrowth around the fundamental signal owing to the IMDs. As discussed earlier, both the digitally controlled feed-forward harmonic cancellation and DPD requires modeling of PA nonlinearity. In order to model this nonlinearity, a system is required to capture harmonics as well as the fundamental signal with IMD components. Based on these captured harmonic components, a behavioral model of PA nonlinearity is first developed, which will produce the correct injected signals for feedforward harmonic cancellation. In general, these injected signals are inverted replica of the harmonics generated by the PA, and an appropriate amplitude and phase calibration can help in canceling PA harmonics using these injected signals.

Similarly, the fundamental signal with IMD components captured is used to generate inverse model for DPD application. Fig. 9 shows the block diagram of filter-less transmitter with provision for capturing non-linear distortion

components. One can see that there is an observation receiver for capturing fundamental signal with IMDs and harmonic components generated by the PA. These signals are captured at the output of PA using a low-loss coupler and received using the receiver in the transceiver board. The LO of the receiver can be tuned to capture either fundamental with IMD components or harmonics one by one for behavioral modeling. An AD-FMCOMMS5-EBZ transceiver board from Analog device is one of the options which have been used in this work [17]. This transceiver board has multiple AD9361 agile radio transceivers chips, which are synchronized with the same baseband clock.

The models generated using the training data from these captured signals can be implemented in the digital domain for feed-forward cancellation and DPD. The original baseband signal, when processed through these models in the digital domain, will generate harmonic components for feed-forward signals as well as predistorted signals for IMD cancellation. This is also shown in Fig. 9. One can see that the DPD model is applied in channel transmitting the fundamental signal, whereas, the harmonic generation model is employed in the baseband of the auxiliary transmitter path used for feed-forward cancellation. Since the feed-forward cancellation and DPD both are open-loop systems; therefore, instant capturing of the fundamental with IMD components and harmonics may not be required. One can generate respective models

off-line and can implement/update them in a regular interval of time. It is worth mentioning that there should be no interruption in transmission while generating and updating these off-line models.

The following sections discuss behavioral modeling of nonlinear distortions and harmonics of PA using NN.

A. BEHAVIORAL MODELING OF DISTORTION AND HARMONICS OF PA USING NEURAL NETWORK

The baseband input signal described as $V_{in} = I + jQ$ is fed at the input port of the PA. The I and Q are the in-phase and quadrature-phase of the input signal. Here, a 5MHz LTE signal with PAPR of 9.5 dB is used as the input signal.

The receiver captures the amplified output of the PA. The relation between output V_{out} and the input baseband signal V_{in} is given as

$$V_{out} = G(V_{in}) \qquad (1)$$

where G is the gain of the PA. It is a complex entity which represents the amplitude and phase change in the modulated output signal corresponding to the amplitude of the baseband input signal. Ideally, G should be constant with the input voltage drive. However, in the practical scenario, the PA operation is nonlinear, introducing gain and phase distortions represented by its AM/AM and AM/PM characteristics, which is shown in Fig. 10. Fig. 10(a) represents the non-linear gain response, which is called AM/AM distortion. This is due to PA's nonlinearity. Fig. 10(b) shows the phase difference between the output signal and the input signal, which is called AM/PM distortion. These non-linear gain and phase compression characteristics will produce IMD as well as harmonics, which depends on the input signal power. For modeling of these harmonics and IMD's, the output of PA is captured, as shown in Fig. 9. The modeling process is a two step approach (1) delay compensation and (2) NN modeling, which is discussed below in detail.

1) TIME DELAY COMPENSATION AND ALIGNMENT

For inverse modeling, accurate time delay compensation is required. Therefore, time alignment is performed using the frequency delay method [18]. Let $x(n)$ is the input signal, $y(n)$ is the output signal. Similarly, y_n is the nth output harmonic, and the corresponding time aligned input signal x^n is obtained by n^{th} exponent of the input signal x. The cross-correlation is given by:

$$F\left(x^n * y_n\right) = F\left(x^n\right) \cdot F\left(y_n\right) \qquad (2)$$

where F represents the Fourier transform and (2) can be rewritten as:

$$F\left(x^n * y_n\right) = K \cdot F\left(x^n\right) \cdot F\left(y_n\right) e^{j(2\pi f \tau + \varphi)} \qquad (3)$$

where K is the gain, τ is the time delay, φ is the phase rotation of harmonic with respect to x^n. The value of cross-correlation in (3) is maximum when $2\pi f \tau + \varphi = 0$. Thus, the time adjusted signal is given as:

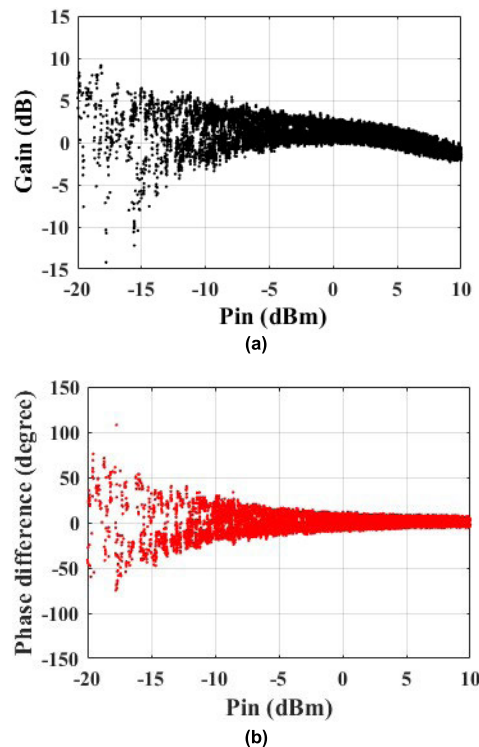$$y_{adj} = y_n e^{-j(2\pi f \tau + \varphi)} \qquad (4)$$

FIGURE 10. Measured (a) Gain distortion (b) Phase distortion with input power.

where n is set to 1 for the fundamental signal, whereas for the 2nd and the 3rd harmonic it should be set to 2 and 3 respectively.

2) NEURAL NETWORK FOR MODELING

The RVFTDNN topology is shown in Fig. 11. This NN topology is a black-box modeling approach and can model the complex signal along with other impairments. When a PA is operating in the nonlinear region, there is significant distortion in the output I/Q data. Besides distortion due to PA, there is also a possibility of impairments like DC offset and I/Q imbalance due to the transmitter. Therefore, to overcoming these types of imperfection, the NN algorithm is used, which is capable of modeling DC offset, I/Q imbalance, and nonlinearities, as shown in Fig. 11 [19].

The feed-forward neural network (FFNN) is a popular tool for modeling, which has an input vector signal of the order $1 \times 2(p + 1)$ as shown in Fig. 11. This input vector signal contains the real value of present and previous input signals, which is given by

$$X(n) = [I_{in}(n), I_{in}(n-1)\ldots\ldots I_{in}(n-p),$$
$$Q_{in}(n), Q_{in}(n-1)\ldots\ldots Q_{in}(n-p)]. \qquad (5)$$

where n is the present training sample and p is the memory length of the FFNN network. The resultant output vector is represented as

$$Y(n) = [I_{out}(n), Q_{out}(n)] \qquad (6)$$
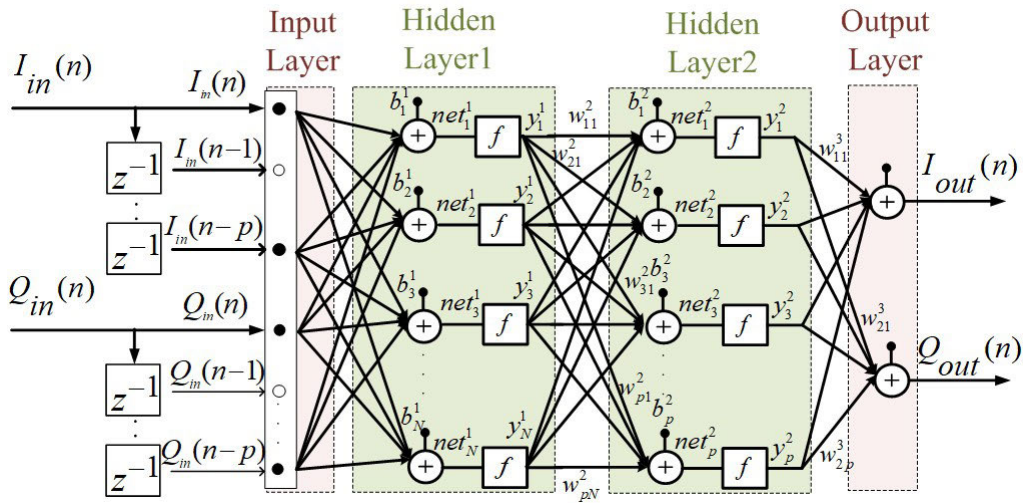
FIGURE 11. Architecture of RVFTDNN.

where $I_{out}(n)$ and $Q_{out}(n)$ are the real and imaginary parts of the output $Y(n)$, respectively.

3) FORWARD COMPUTATION

The feed-forward mechanism is used in RVFTDNN, which is shown in Fig. 11. In this figure, there are three types of layers: (a) input layer (b) output layer (c) hidden layer. The hidden layers are connected to each other as well as to the input and output layers. During forward computation, the input data to the next hidden layer $(k+1)^{th}$ is calculated by using the output of the present layer $(k)^{th}$ multiplied with the weights (w_{ij}^{k+1}). This is represented by

$$\text{net}_i^{k+1} = \sum_{j=1}^{N} w_{ij}^{k+1} y_j^k + b_i^{k+1} \tag{7}$$

where net_i^{k+1} is the ith neuron of $(k+1)^{th}$ layer. N denotes the total number of neurons in the present layer $((k)^{th}$ layer), w_{ij}^{k+1} represents the synaptic weight connecting the ith neuron of the next $((k+1)^{th})$ layer to j^{th} output (y_j^k) of the present $((k)^{th})$ layer. b_i^{k+1} indicates the bias of ith neuron of $(k+1)^{th}$ layer. The output of ith neuron of $(k+1)^{th}$ layer can be calculated as:

$$y_i^{k+1} = f(\text{net}_i^{k+1}) \tag{8}$$

where f is a nonlinear activation function (hyperbolic tangent function), which maps the nonlinearity between -1 and 1. Initial weights are chosen randomly, which converse iteratively towards their optimum output.

4) BACKWARD COMPUTATION

The backward computation is used for error calculation between the desired output and the estimated output of NN. This error will train the data in order to minimize the error between computed and desired output. The error energy

(cost function) in forwarding pass is given by

$$\Psi = \frac{1}{2N} \sum_{n=1}^{N} \{[I_{out}(n) - \hat{I}_{out}(n)]^2 + [Q_{out}(n) - \hat{Q}_{out}(n)]^2\} \tag{9}$$

where ψ is the total mean square error, $\hat{I}_{out}(n)$ and $\hat{Q}_{out}(n)$ are the calculated estimated output using forward computation, $I_{out}(n)$ and $Q_{out}(n)$ are the desired output pairs. Assuming δ_i^k as the local gradient for the ith neuron of kth layer, it can be written as (10)

$$\delta_i^k = e_i^k f'(\text{net}_i^k) \quad k = \text{Present Layer} \tag{10}$$

$$e_i^k = \begin{cases} t_i - y_i^k, & k = \text{Output Layer} \\ \sum_{j=1}^{N_{k+1}} w_{ij}^{k+1} \delta_j^{k+1}, & k = \text{Hidden Layer} \end{cases} \tag{11}$$

where e_i^k is the error term for the ith neuron in the kth layer and $f'(\text{net}_i^k)$ is the 1st derivative of the activation function. For finding the convergence condition, one must minimize the error energy, which is given in (9). The backward computation is responsible for adjusting the bias and synaptic weights of the network. For weight updation of each layer, several well defined numerical optimization techniques have been used in past such as gradient descent (GD) method, resilient propagation (RP) method, conjugate gradient (CG) method, Fletch-Reeves version of conjugate gradient (CGF), Levenberg Marquardt (LM) method, etc. [20]–[23]. The performance of the different algorithms for forward modeling of harmonics is studied in the same situation (assuming 2 hidden layers and each has 8 neurons) for the same input training data. The cost of different algorithms in terms of mean squared error is shown in Fig. 12. One may conclude that Levenberg Marquardt (LM) algorithm has lowest cost function and highest convergence rate. So, in this paper, the LM algorithm is used. This algorithm is a numerical optimization of the Gauss-Newton method [24]. The weight update equation of LM algorithm at $(i+1)^{th}$ iteration can be
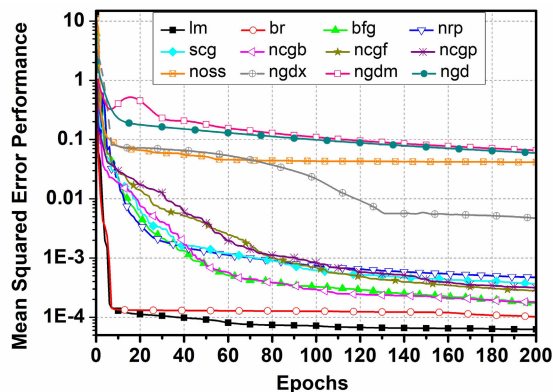
*lm: Levenberg-Marquardt, br: Bayesian Regularization, bfg: BFGS Quasi-Newton, nrp: Resilient Backpropagation, scg: Scaled Conjugate Gradient, ncgb: Conjugate Gradient with Powell/Beale Restarts, ncgf: Fletcher-Powell Conjugate Gradient, ncgp: Polak-Ribiére Conjugate Gradient, noss: One Step Secant, ngdx: Variable Learning Rate Gradient Descent, ngdm: Gradient Descent with Momentum, ngd: Gradient Descent.

FIGURE 12. Convergence of various NN optimization algorithm for forward modeling of harmonics of PA.

written as

$$W_{(i+1)} = W_i - [J^T(X)J(X) + \mu I]^{-1}J^T(X)e(X) \qquad (12)$$

$$e(X) = [e_I(1)e_Q(1)e_I(2)e_Q(2), \ldots \ldots \ldots e_I(N)e_Q(N)] \qquad (13)$$

where $J(X)$ is the Jacobian matrix of performance calculated using input vector X, W is NN coefficient matrix for any layer given as

$$W = [w_{11}^{k+1} \ w_{12}^{k+1} \ldots \ldots w_{ij}^{k+1} \ b_1^{k+1} \ldots .b_i^{k+1}] \qquad (14)$$

where w_{ij}^{k+1} and b_i^{k+1} denotes number of weights and biased respectively for any layer. In (12), I denotes the identity matrix, and μ represents the step size for the weight update equation. A very high value of μ provides the steepest descent solution, whereas a small value of μ leads to Gauss-Newton solution, which avoids falling into local minima. In this algorithm, firstly, the network parameters are initialized. Then the average sum of square error is computed using (9). The updation of weights takes place by calculating the Jacobian matrix and the error gradient vector. After this step, the network parameters are updated, and the mean square error is computed. If the mean square error is greater than the previous step, then the initial value of weight vector has to be changed. Otherwise, if the mean square error is found to be less than its previous value, the weight vector is adopted, and μ is stepped down for the next iteration. This training will continue for several iterations until the desired performance is achieved. The convergence curve with the iterations is shown in Fig. 12. The convergence is also depends on the number of neurons that exists in the hidden layers in RVFTDNN. The effects of number of neurons in convergence for the same training data and same condition (number of Epochs = 200, and number of hidden layers = 2, each layer has same neurons) is shown in Fig. 13.
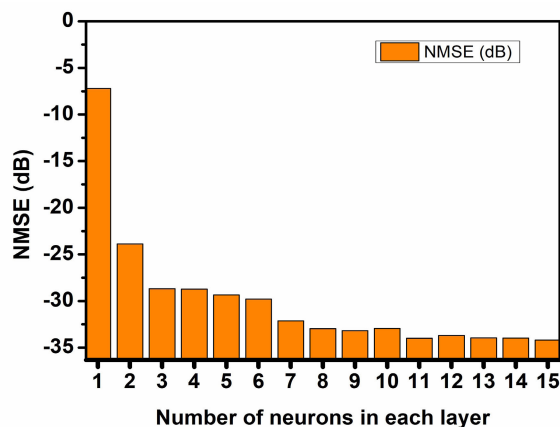

FIGURE 13. Convergence of model with respect of number of neurons in the each layer.
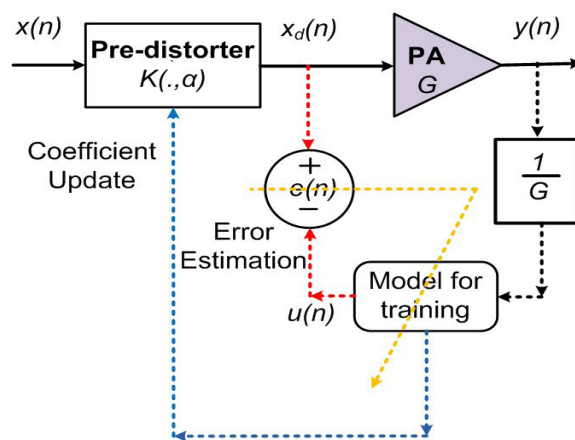

FIGURE 14. The architecture of DPD using ILA.

One may have depicted that after the eight neurons, the performance is not effected much. So, in this paper, 8 neurons in 2 hidden layers are used for modeling of harmonics and IMD's.

B. INVERSE MODELLING FOR PREDISTORTION

The distortion characterization and harmonic cancellation setup is shown in Fig. 9. The predistortion scheme requires a behavioral model of the distorted captured signal. Then the inverse of this model is implemented in the digital domain to predistorter the signal, which is fed to the transceiver board. This whole technique is known as Indirect Learning Architecture (ILA) [25], [26]. Fig. 14 shows the architecture of ILA. One can see, $x(n)$ is the input signal to the predistorter. This predistorted output is represented as $x_d(n)$, which is the input signal for PA. The amplified output $y(n)$ is scaled down by a factor G $(y(n)/G)$ in the feedback path for modeling of predistorter. In this iteration, the output of model $(u(n))$ is compared with the input signal of PA $x_d(n)$, which generates the error estimation signal $e(n)$. This $e(n)$ will train the predistorter model. The predistortion model is updated in each iteration until the desired NMSE is achieved.

In the first iteration, the predistortion has no data to process. Thus, whatever input is given to the predistorter will appear at the output in the same form.

$$X_d(n) = x(n) \tag{15}$$

$$u(n) = \xi[y(n)/G] \tag{16}$$

Ideally, assuming that predistorter is perfect, $u(n)$ should be equal to $x(n)$, therefore inverse modeling requirement becomes

$$x(n) = \xi[y(n)/G] \tag{17}$$

$x(n)$ and $y(n)$ are the known data from measurement. The nonlinear predistortion model coefficient of ξ can be estimated with the help of adaptive digital signal processing (ADSP).

In this paper, the feed-forward NN (FFNN) is used to calculate the ξ. For calculating the optimum number of neurons and optimization algorithm, analysis similar to previous section is carried out. Since, the DPD based on NN is well-established [9], [18], [19] the details are not included here. Once coefficients of the model are extracted from the input and output of PA, they are updated in the predistorter in the digital domain.

The distortion mitigation potential of a digital predistortion technique depends on the accuracy of the model, which is trained to learn the inverse characteristic ξ as given in (17). The performance of any model can be defined in term of normalized mean-square error (NMSE) expressed as

$$\text{NMSE} = 10 \log_{10} \left(\frac{\sum_{i=1}^{N} (\hat{I} - I)^2 + (\hat{Q} - Q)^2}{\sum_{i=1}^{N} I^2 + Q^2} \right) \tag{18}$$

where I/Q are the desired output values of the model and $\hat{I}/\hat{Q}$ are the predicted output values from the model.

NN is a black box modeling technique capable of modeling any data. Thus, for modeling of fundamental distortion and harmonic signal, NN based model is used in this paper. In this model, after the extraction of the weights for the NN based predistorter, the original baseband signal (I and Q) is passed through a predistorter. The output of the distorter is fed at the input of the PA. This pre-distorted signal is trained to compensate the interference and nonlinear distortion. In an ideal case, the predistorter is nothing but an inverse function of non-linearity and interference. Thus, the output signal from the pre-distorter is free from all types of distortion.

As similar to predistorter, the NN is applied for modeling of harmonic signal. This modeled out-of-phase harmonic signal is passed through the auxiliary branch to cancel out the harmonic of PA.

The level of suppression of distortions in fundamental component and cancellation of harmonics depend on the accuracy of a model, which is measured in terms of NMSE. In this paper, NMSE of the model is observed around -30dB.

V. BENCHMARKING FILTER-LESS TRANSMITTER WITH THE STATE OF ART

The filter-less transmitter architecture has the main advantage of frequency agility and miniaturized solution in VHF/UHF bands, particularly suitable for SDR application. For linearization such as IMD cancellation, both the architectures require digital signal processing such as DPD. The filter-less transmitter architecture utilizes this unavoidable signal processing for harmonic cancellation by incorporating some additional digital functionality. There are several limitations in the conventional transmitter using a switched filter bank, which can be alleviated using filter-less transmitter architecture, as discussed in the following section.

A. LIMITATIONS OF TRANSMITTER USING SWITCHED FILTER BANK AND THEIR SOLUTION

The switched filter bank based architecture has limited flexibility of channel selection and availability of the number of channels within the operating bands. In switched filter bank, each channel is set such that the 2nd harmonic of its operating range should not fall within the channel. Otherwise, harmonics will not be suppressed. Therefore, the number of channels in the switched filter-bank is decided by the lowest and highest frequency of operation. For example, a commercial switched filter bank has an operating frequency range from 50MHz-500MHz [27]. There are six channels available for transmission in this switched filter bank. Channel 1 has a frequency range from 50 MHz-75 MHz, whereas channel 2 has a transmission band from 70 MHz-100 MHz. Similarly, channels 3, 4, 5, and 6 have transmission bands of 95 MHz-150 MHz, 145 MHz-200 MHz, 195 MHz-300 MHz, 295 MHz-500 MHz respectively.

In the case where only limited harmonics are required to be handled (e.g. 2nd and 3rd only) these several channels unnecessary increases complexity in terms of the number of filters and switches. Moreover, due to the high roll-off of the filters, there is no flexibility of transmitting 10 MHz LTE signal at corner frequencies of these channels i.e. 72.5 MHz, 97.5 MHz, 147.5 MHz, 197.5 MHz, and 297.5 MHz. Moreover, it is not possible to transmit signals with a high bandwidth (e.g. 30 MHz) even at several frequencies falling within transmission bands of each channels. For example, it is not possible to transmit a 30 MHz LTE signal in channel 1 due to its limited bandwidth. Even with the bandwidth availability in other channels, this 30 MHz LTE cannot be transmitted seamlessly at any frequency of transmission channel. For example, channel 2 can transmit this 30 MHz signal only at 85 MHz carrier frequency. Similarly, this 30 MHz signal can only be transmitted at carrier frequencies ranging from 110 MHz-135 MHz in Channel 3, 160MHz-185MHz in Channel 4, 210MHz-285MHz in Channel 5 and 310MHz-485 MHz in channel 6. Therefore, all the frequencies defined in each transmission channel in case of switched filter-bank may not be available for transmitting broadband signals. Besides, if new frequency planning is required in the

transmitter with channels at different frequencies, entirely new switched filter-banks has to be developed. However, this is not the case for the filter-less transmitter, where, one can digitally generate harmonics and transmit fundamental signal seamlessly over the entire frequency range of the transmitter.

In the case of switched filter banks with narrow channels as discussed above, a high roll-off is required. This eventually increases the numbers of resonators in the filter architecture in each channel, thereby increasing the loss and resulting in complex and bulky architecture. The filter-less architecture requires a broadband combiner. In the case of harmonic injection, the two signals which are combined are not at the same frequency; instead, they are at two different frequencies. In such a case, if all the harmonics fall out of band, a diplexer/multiplexer can provide an easy solution with low loss. These diplexers/multiplexers also use filters in each path to suppress the leakage from the other path. However, in the case of multi-octave transmitters, where harmonics lie within the band, it is not possible to use diplexers/multiplexers. This is because the harmonics for one frequency can be the same as another operating frequency. Therefore, a diplexer designed for one fundamental frequency may not be useful for another operating frequency. In such a case, this work uses a wideband Wilkinson power combiner. This combiner, although, provides a minimum 3 dB insertion loss for the entire multi-octave range, it can seamlessly handle any operating frequency and its harmonics over the whole multi-octave frequency range. In the case of the switched filter bank, the loss may be high, typically around 5-6 dB based on the number of transmission channels and how closely they are placed [27]–[30]. It is worth mentioning that due to the use of EA in filter-less transmitters, its power consumption is similar to the architecture using switched filter-bank with higher loss. Yet, it is alleviating several limitations in conventional architecture using a switched filter bank.

In addition, the switching architecture of switched filter bank restricts concurrent multi-band transmission where the two modulated signals are transmitted concurrently at two carrier frequencies. This is because the switching configuration will only allow the selection of one channel at a time. However, the filter-less architecture has no such limitation and can transmit multiple carriers concurrently at any frequencies over the operating range. This is because harmonics are generated digitally and their feed-forward addition to the PA output, will cancel the harmonics of the PA.

B. COMPARISION OF NN MODEL WITH THE EXITING HARMONIC RELATED SOLUTIONS

In the literature, [9]–[15] explore the cases related to harmonic interference. The works reported in [9]–[11] use a feed-forward harmonic cancellation technique for harmonic suppression. All these works use additional reference signals at the input of the PA for harmonic modeling. These signals, although small in the amplitude, are injected at the input of PA for estimating the time delay of harmonic signals appearing at the output of the PA. The output harmonic signals are

TABLE 1. Coefficient comparison between various harmonic models.

	Model	Total Number of Coefficient	Reported coefficients
[12],[14]	2D-HMP	$0.5*[(M+1)+(M_l+1)*Q_l + (M_u+1)*Q_u]*(K+1)*(K+2)$	540 (For $Ml=Mu=4$, $Ql=Qu=7$)
[13]	2-D MP	$(K+1)*(K+2)*(M+1)$	112* (For $K=6$, $M=1$)
[15]	3D-HMP	$2.5*(K+1)*(K+2)*M*K$	3360 (For $M=4$, $K=6$)
[This work]	RVFTDNN	$2*(M+1)*p+p*q+2*q+p+q+2$	162 (For $p=q=8$; $M=3$)

Q_l/Q_u: IMD product orders; M_l/M_u: memory depth; K: nonlinearity order; M: memory depth; p: Number of neurons in the first layer; q: Number of neurons in the second layer.
* Not mentioned assuming same as [9].

cross-correlated with their corresponding reference signals to obtain the time delay, which must be adjusted to model the harmonics. Therefore, in such cases, the signals are injected at both the input (for time alignment during modeling) and the output (for feed-forward cancellation) at harmonic frequencies. In the case of narrowband DACs, this requires more auxiliary paths for injecting signals at the input as well as the output of the PA, making the system more complex and bulky. As the number of harmonics increases, this complexity increases further.

The characterization of harmonics in such cases also requires extra processing and may add to power consumption in the case of high power transmitters. On the contrary, the proposed scheme trains the NN model for capturing the harmonic behaviour of PA without the requirement of any additional reference signal. This is one crucial feature of the proposed NN model, which undoubtedly reduces the hardware complexity in the filter-less transmitter.

The work reported in [12]-[15] cater to the unique scenario of concurrent multi-band transmission where signals transmitted in second or third band falls over the 2nd and 3rd harmonics of the signal transmitted in the first band. In such a case, the signals transmitted at second and third bands concurrently acts as reference signals for 2nd and 3rd harmonics of the signal transmitted at the first band. Therefore, the harmonics of the signal transmitted at first band can be modeled without injecting any additional reference signal. One should understand that this is a specific scenario and it is rare that every time the concurrent multi-band transmission happens in harmonically related frequencies. Considering the scenario, where no additional reference signal is added at the input of PA, the Table 1 compares the complexity in terms of the number of coefficient of the harmonic models available in the state of the art. From the above table, one can see that proposed RVFTDNN model has low complexity in terms of number of coefficient of 2 dimensional harmonic memory polynomial (2D-HMP), and 3 dimensional harmonic
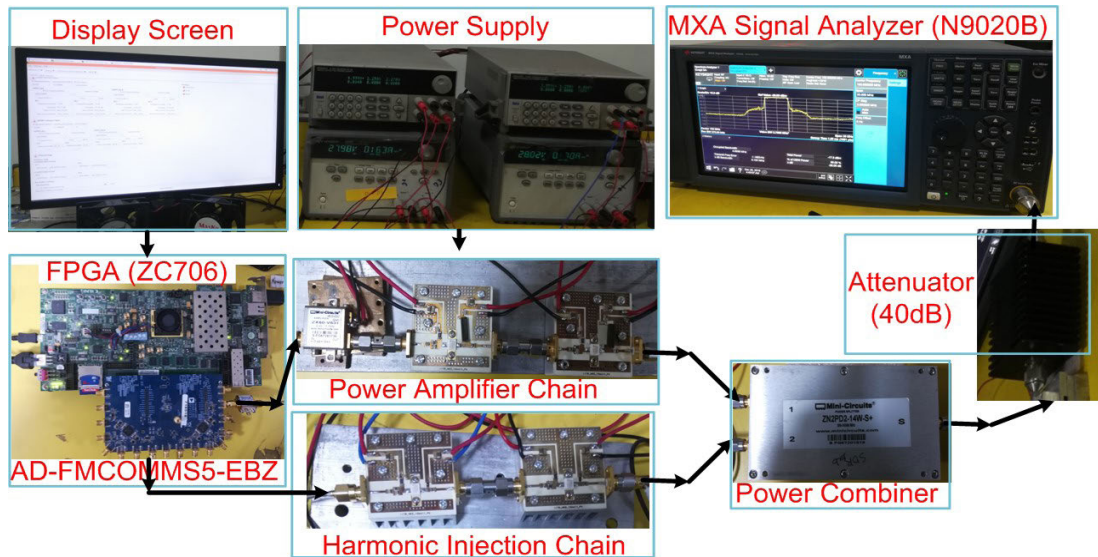
FIGURE 15. Hardware setup implementing the filter-less architecture of PA.

memory polynomial (3D-HMP) models in [12], [14]–[15]. Whereas, number of coefficients of proposed RVFTDNN are comparable to the 2 dimensional memory polynomial (2D-MP) reported in [13]. In addition, RVFTDNN based model can easily handle other transmitter's impairments such as crosstalk, I/Q imbalance, and dc offsets. In fact, it has been established in the literature that a single NN can compensate for all the transmitter impairments [31].

Moreover, NN is an iterative method; therefore, its main advantage is in terms of model training for adaptive modeling applications. For the slow dynamic effects such as a change in environmental conditions, the training of the model can be done intermittently after a fixed time interval in offline mode. The trained models can then be updated without disturbing the transmission. The fast dynamic effects, such as memory effect, can be compensated within NN modeling by training the model for instantaneous as well as past samples. Moreover, with slow changes such as thermal conditions, the NN architecture (number of weights and layers) remains the same, only the values of weights and bias updates. Therefore, the already trained model of NN can update very fast for accommodating slow changes such as thermal.

Also, NN models are generally backward compatible as compared to other polynomial models, even with the change in input signals [31]–[33]. Therefore, in terms of complexity, processing, performance, and adaptability, NN based algorithm is an excellent choice for harmonic modeling and DPD in transmitters [31]–[33].

VI. MEASUREMENT SETUP AND MEASURED RESULTS OF PREDISTORTION AND HARMONIC CANCELLATION

The proposed filter-less transmitter is realized using a low-cost SDR platform comprises of embedding platform ZC706 [34] along with a digitally reconfigurable transceiver board (AD-FMCOMMS5-EBZ) from Analog

Devices. Fig. 15 shows the hardware setup implemented for the proof of concept. The transceiver board utilizes a reconfigurable radio chip AD9361 with DAC operating at a sampling rate of 61.44 MSPS. The reconfigurability can be digitally controlled using the ARM processor in ZC706. The radio chip AD9361 also upconverts the baseband signal using QMD, and a gain block following it provides gain to the upconverted signal. The transceiver board AD-FMCOMMS5-EBZ has two AD9361 chips, which are synchronized with the same baseband clock. This makes it quite suitable for filter-less transmitter applications, where multiple transmitter paths are required for feed-forward harmonic cancellation. Similarly, one of the receivers of FMCOMMS5-EBZ is used to capture a fundamental signal with IMD and harmonics, as shown in the block diagram of Fig. 9.

One can see from Fig. 15 that there are two branches of PA. The first branch consists of the PA chain comprising of cascaded driver stages and PA. The second branch consists of EA for adjusting the power level of the injected harmonic signals in the feed-forward path for harmonic cancellation. Since the injected harmonics are generated digitally using the NN based harmonic model, one can tune the phase and amplitude of each injected harmonic components digitally. This can be performed in baseband by multiplying different complex gain values to each harmonic component. In addition, the AD9361 transceiver chip also has the provision of gain control, which can also be used for tuning the amplitudes of harmonics precisely. The EA will provide amplification to the power levels of these harmonics such that they can compensate for the harmonics generated by the PA. The EA should be designed to linearly amplify the harmonics to the required power levels. As shown in Fig. 8, the 2nd and 3rd harmonics are inherently suppressed below -15 dBc over the frequency range. Therefore, the output power required from EA is typically 15 dB below the output power of PA. To ensure the
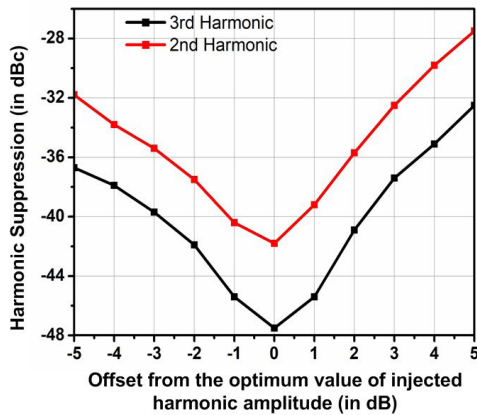
FIGURE 16. Variation in magnitude of harmonics suppression with variation in the power of the injected harmonic signal.
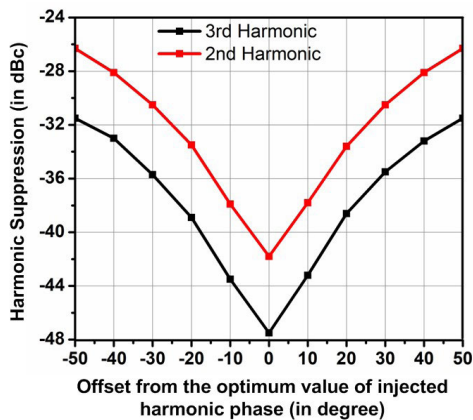

FIGURE 17. Variation in magnitude of harmonics suppression with variation in the phase of the injected harmonic signal.

FIGURE 18. Measured output spectrum with/without DPD and harmonic injection @100MHz.

linearity, the EA must be operated 10-15 dB back-off from its saturation. Therefore, in this case, the EA comprises of two cascaded amplifiers using 10-watt Cree device CGH40010 as shown in Fig. 15. Although having similar topology as the main PA, the EA operates at back-off to ensure linear operation. Therefore, its power consumption is far less as compared to the main PA. The cancellation of harmonics at the output of PA depends on the appropriate amplitude and phase of the injected harmonic signal. Fig. 16-17 shows the sensitivity of the setup with the amplitude and phase of the injected harmonic signal, respectively. Fig. 16 shows the variation of the amplitude of injected signals from its optimum value. One can see that the best harmonic suppression values for the 2nd and 3rd harmonics are around −42 dBc and −48 dBc, respectively. These are obtained at 0 offsets from the optimum amplitude value. However, at ±2 dB offset, the 3rd harmonic suppression reduces to around −42 dBc/−40 dBc. Similarly, for the same variation in amplitude level from its optimum value, the 2nd harmonic suppression reduces to around −37 dBc/−36 dBc.

Fig. 17 shows the harmonic suppression with the variation in the phase of the injected signal from its optimum value. One can see that the respective maximum value of harmonic
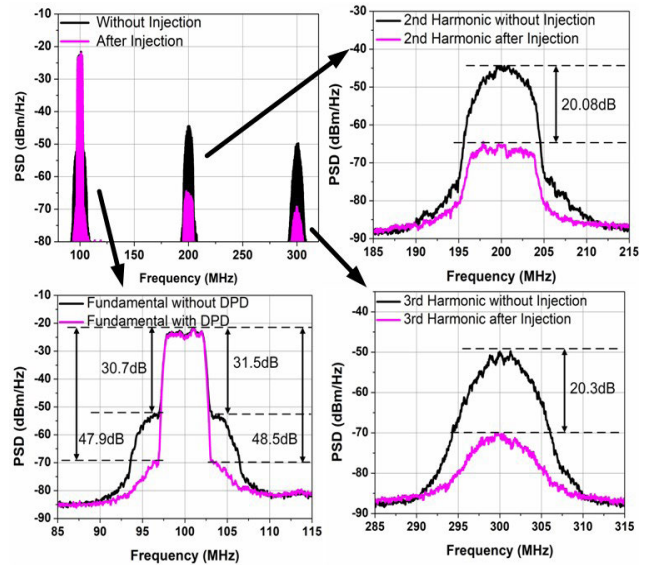
suppression is achieved as −42 dBm and −48 dBm for the 2nd and 3rd harmonics at 0° offset from the optimum value. However, at ±10° variation in phase from this optimum value, the 2nd and 3rd harmonic suppression reduces to around −38 dBc and −44 dBc, respectively.

One can conclude from Fig. 16 and 17 that the proposed scheme is robust and less sensitive to even high amplitude and phase variation. This depends on the accurate modeling of harmonic, as discussed in this paper.

Figs. 18-21 show the results of harmonic suppression due to digital feed-forward cancellation for various frequencies over the operating band of the PA. These figures also report the adjacent channel leakage suppression due to DPD. One can see from Fig. 18, that fundamental signal is at 100 MHz, whereas its 2nd and 3rd harmonics are at 200 and 300 MHz, respectively. Without any harmonic injection, the 2nd harmonic suppression was −22.87 dBc. However, after injecting harmonic at the appropriate amplitude and phase from the auxiliary channel, the harmonic suppression reaches to −42.95 dBc. This corresponds to an improvement of 20.08 dB. Similarly, the 3rd harmonic was initially suppressed to −28.18 dBc and improved to −48.5 dBc with harmonic injection. Fig. 20 also shows the ACLR (L/U) of −30.7/−31.5 dBc without applying DPD. The L/U represents the ACLR at the lower and upper band around the carrier, respectively. After applying the DPD, the ACLR (L/U) improves to −47.9/−48.5 dBc. This corresponds to an improvement of around 17 dB in ACLR when DPD is applied.

Fig. 19 shows the case when fundamental is applied at 200 MHz and corresponding 2nd and 3rd harmonics are generated at 400 MHz and 600 MHz. One can see that the adjacent channel leakage ratio ACLR (L/U) of −31.5/ −31.4 dBc without applying DPD. However, after applying the DPD, the ACLR improves to −46.6 dBc in both lower and upper bands around the carrier. This corresponds to an
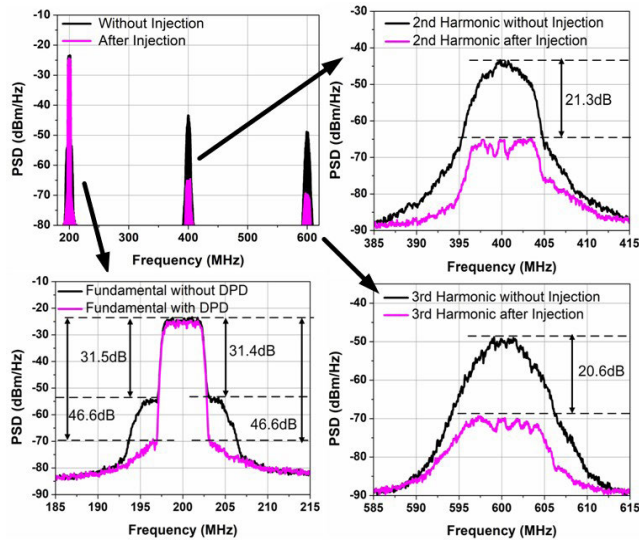
FIGURE 19. Measured output spectrum with/without DPD and harmonic injection @200MHz.
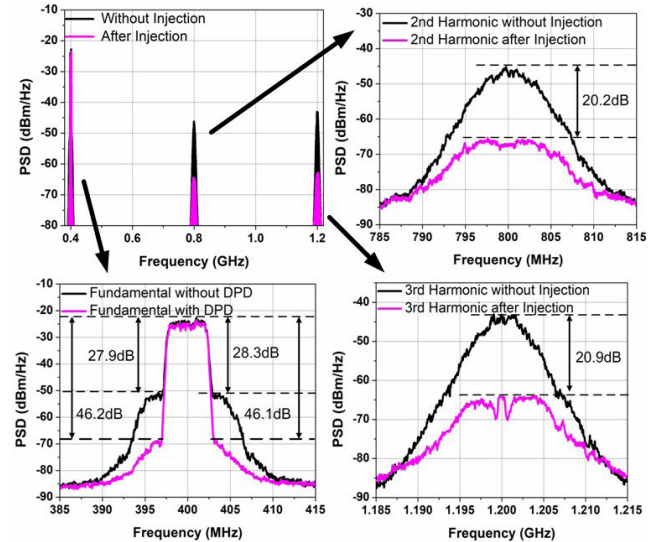

FIGURE 20. Measured output spectrum with/without DPD and harmonic injection @300MHz.

FIGURE 21. Measured output spectrum with/without DPD and harmonic injection @400MHz.
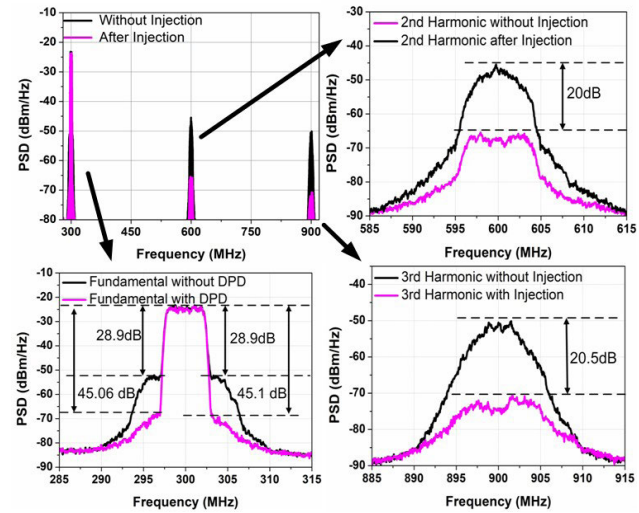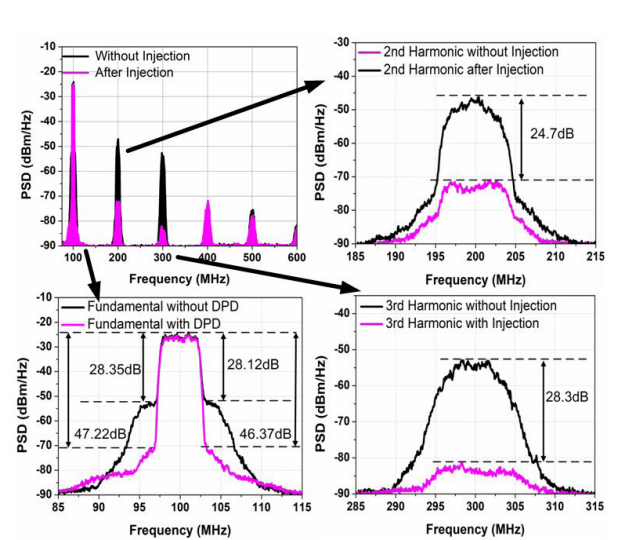

FIGURE 22. Measured output spectrum with/without DPD and harmonic injection simultaneously using AWG5204 @100MHz.

improvement of around 15.1 dB in ACLR when DPD is applied. Similarly, the 2nd harmonic suppression improves from −19.99 dBc to −41.29 when harmonic is injected with feed-forward cancellation. This shows an improvement of 21.3 dB in harmonic suppression with the proposed scheme. Fig. 21 also shows 3rd harmonic suppression which improves from −25.45 dBc to −46.05 after injecting harmonic for the proposed feed-forward cancellation. This corresponds to an improvement of 20.6 dB.

Fig. 20 shows the transmission of the fundamental frequency at 300 MHz, where the 2nd and 3rd harmonic appear at 600 MHz and 900 MHz, respectively. One can see that the 2nd harmonic suppression was −22.27 dBc without any harmonic injection. However, after injecting harmonic at the appropriate amplitude and phase from the auxiliary channel, the harmonic suppression reaches to −42.27 dBc. This corresponds to an improvement of 20 dB. Similarly, the 3rd harmonic

suppression improves from −26.94 dBc to −47.44 when harmonic is injected with feed-forward cancellation. This shows an improvement of 20.5 dB in harmonic suppression with the proposed scheme. Fig. 22 also shows the adjacent channel leakage ratio ACLR of −28.9 dBc in both the lower and upper band around the carrier without applying DPD. However, after applying the DPD, the ACLR improves around −45 dBc. This corresponds to an improvement of around 16.1 dB in ACLR when DPD is applied.

Fig. 21 shows the case when fundamental is applied at 400 MHz, and corresponding 2nd and 3rd harmonics are generated at 800 MHz and 1200 MHz. One can see that the adjacent channel leakage ratio ACLR (L/U) is −27.9/−28.3 dBc without applying DPD. However, after applying the DPD, the ACLR improves around −46.1 dBc in both lower and upper bands around the carrier. This corresponds to an
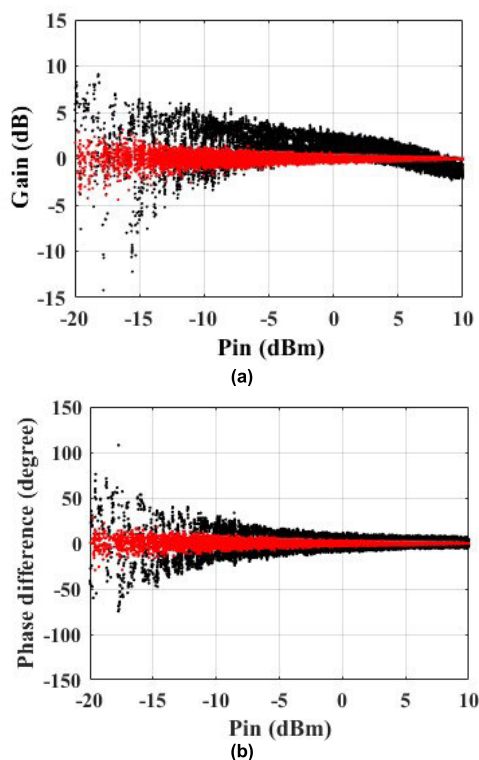
FIGURE 23. Measured results of power amplifier with/without DPD correction (a) AM/AM distortions (b) AM/PM distortions.

improvement of around 17.9 dB in ACLR when DPD is applied. Similarly, the 2nd harmonic suppression improves from −22.42 dBc to −42.62 dBc when harmonic is injected with feed-forward cancellation. This shows an improvement of 20.2 dB in harmonic suppression with the proposed scheme. Fig. 23 also shows 3rd harmonic suppression, which improves from −20.29 dBc to −41.19 after injecting harmonic for the proposed feed-forward cancellation. This corresponds to an improvement of 20.9 dB.

It is worth mentioning that although the AD-FMCOMMS5-EBZ board used in the proposed scheme has four transmitting channels, however, there are only two LOs which can be independently tuned. Therefore, it is able to transmit signals at only two different frequencies in its four transmitter channels. Also, each transmitter channel has limited bandwidth hence it is difficult to transmit all the harmonics through one auxiliary channel. Therefore, the same auxiliary channel is used for injecting 2nd and 3rd harmonic one by one in the off-line mode for the proof of concept. However, to validate the proposed scheme for simultaneous cancellation of 2nd and 3rd harmonic along with ACLR reduction using DPD, an instrument based testbed is developed using high bandwidth DACs available in Arbitrary waveform generator (AWG) 5204 from Tektronix. This AWG has four channels with wideband DACs out of which two channels are used. One channel transmits a fundamental LTE signal of 5 MHz at 100 MHz carrier frequency and the other channel concurrently transmits 2nd and 3rd harmonics. The EA and power combiner used are the same as used previously. Fig. 22 shows the measured output spectrum

with harmonic cancellation as well as linearization. One can see from Fig. 22, that fundamental signal is at 100 MHz, whereas its 2nd and 3rd harmonics are at 200 and 300 MHz, respectively. Without any harmonic injection, the 2nd and 3rd harmonic suppression was −22.15 dBc and −28.8 dBc respectively. However, after injecting simultaneously 2nd and 3rd harmonic at the appropriate amplitude and phase from the auxiliary channel, the harmonic suppression reaches to −46.85 dBc and −57.2 respectively. This corresponds to an improvement of 24.7 dB in 2nd harmonic suppression and 28.3 dB for 3rd harmonics. The amplitude and phase are added by multiplying each injected harmonic signal with appropriate complex gain at baseband. The predistorted signal after DPD is also sent to the PA at the same time through the main path. Without applying the DPD, the ACLR (L/U) were −28.35 / −28.12 dBc which are improved to 47.22/46.37 dBc after applying DPD. This corresponds to an improvement of around 18.2 dB in ACLR when DPD is applied. One can see that the performance is better in term of harmonic suppression as compared to the Figs. 18-21 due due to the use of higher-end instruments.

Fig. 23 shows the AM/AM and AM/PM response for transmitting 5 MHz LTE carrier at 100 MHz before and after employing DPD. One can see 3.8 dB distortion in gain and 13.6° distortion in phase has been corrected after DPD.

The characteristics of the proposed architecture is compared with some related papers in Table 2. The table reports improvement in terms of harmonic suppression using digital cancellation with respect to the inherent harmonic suppression in PA. The schemes proposed in [9], [10] demonstrates compensation of only one harmonic. This is perhaps due to the use of an additional reference signal injected at the input of PA for harmonic modeling. This additional injection increases hardware complexity especially when number of harmonics increases. The proposed NN model-based scheme does not utilize any such reference signal for harmonic modeling, yet its performance is comparable to [9], [10] when the proposed scheme is validated with the instrument-based test-bed.

The work reported in [12]–[15] exhibits good performance and they do not require any injection of reference signal at the input of the PA. However, the proposed scheme is applicable to unique scenario of concurrent multi-band transmitters where concurrent transmission happens at harmonically related frequencies. The results reported in [15] is comparable to the proposed work when it is validated with the instrument-based test-bed. However, the results reported in [12]–[14] are comparable with the proposed scheme even using a low-cost embedded platform.

One can also see from Table 2 that the proposed work demonstrates the performance at high power where the device can produce high level of harmonic power and difficult to cancel. Besides, the proposed architecture is demonstrated at VHF/UHF band with both the harmonics handled by a single auxiliary path. At such low-frequency ranges, the devices have ample gain to produce prominent harmonic components

TABLE 2. STATE OF ART PA for filter-less transmitter.

Reference	[9]	[10]	[12]	[13]	[14]	[15]	This work
2nd H.S.(dB)	26.9	N.P	17.7	16.6*	20.29	25.48	24.7[#]/ 21.3[##]
3rd H.S. (dB)	N.P	31	N.P	N.P	N.P	23.19	28.3[#]/ 20.9[##]
2nd and 3rd simultaneous H.S. with DPD	N.P	N.P	N.P	N.P	N.P	Yes	P[#] /NP[##]
ACLR/ ACPR Correction (dB)	19*	18*	18.5	17.5*	23.3	21.61	18.9[#]/ 18.3[##]
Output power (dBm)	11	11	11	25	11	28.0	39.0

H.S.: Improvement in harmonic suppression w.r.t no digital correction.
P: Performed, N.P: Not performed, * ACLR, **ACPR
*Data are estimated from the figures.
[#]Reported results are from Instrument based testbed.
[##]Reported results are from low-cost transceiver & the embedded platform.

and the RF filters are too bulky to be considered as a good option.

VII. CONCLUSION

This paper presents a new RVFTDNN based model which does not require any reference signal injection at the input of PA for harmonic modeling. This model is generic and can be used for single as well as concurrent multiband transmission at any arbitrary frequencies over the specified operating range of the transmitter. The proposed scheme is validated with the hardware implementation of a multi-octave filter-less transmitter operating at VHF/UHF frequency ranges. The hardware is implemented using an in-house developed PA and a low-cost SDR using agile RF transceiver along with an embedded platform. This feed-forward harmonic compensation is also validated with instrument based test-bed for handling 5 MHz LTE signal transmission with simultaneous compensation of IMD as well as 2nd and 3rd harmonics. The proposed scheme provides good harmonic suppression without any RF filter. Being compact form-factor due to the absence of bulky RF switched filter bank, this architecture can be future for high level of integration in multi-octave transmitter design.

REFERENCES

[1] P. B. Kenington, *RF and Baseband Techniques for Software Defined Radio*. London, U.K.: Artech House, 2005, pp. 1–301.

[2] D. Paunovic, M. Dukic, A. Ratkovic, and I. Stojanovic, "The prediction of the interference and service zones in the VHF/UHF tactical radio systems," in *Proc. Electrotech. Conf. Integr. Res., Ind. Edu. Energy Commun. Eng.*, Lisbon, Portugal, 1989, pp. 441–444.

[3] J. Kim, Y. Kim, S. Oh, J. Choi, D.-H. Lee, K. Cho, S. Lee, and C.-H. Ahn, "A 20 W wide bandwidth GaN HEMT power amplifier for VHF/UHF applications," *IEEE Trans. Ind. Electron.*, early access, Dec. 2019, doi: 10.1109/TIE.2019.2960749.

[4] N. Sahan, M. E. Inal, S. Demir, and C. Toker, "High-power 20–100-MHz linear and efficient power-amplifier design," *IEEE Trans. Microw. Theory Techn.*, vol. 56, no. 9, pp. 2032–2039, Sep. 2008.

[5] S. Pisa, S. Chicarella, R. Cusani, and J. Citrolo, "30-512 MHz power amplifier design using GaN transistor," *Microw. Opt. Technol. Lett.*, vol. 60, no. 5, pp. 1280–1286, May 2018.

[6] P. Roblin, S. K. Myoung, D. Chaillot, Y. G. Kim, A. Fathimulla, J. Strahler, and S. Bibyk, "Frequency-selective predistortion linearization of RF power amplifiers," *IEEE Trans. Microw. Theory Techn.*, vol. 56, no. 1, pp. 65–76, Jan. 2008.

[7] F. M. Ghannouchi and O. Hammi, "Behavioral modeling and predistortion," *IEEE Microw. Mag.*, vol. 10, no. 7, pp. 52–64, Dec. 2009.

[8] J. Xu, W. Jiang, L. Ma, M. Li, Z. Yu, and Z. Geng, "Augmented time-delay twin support vector regression-based behavioral modeling for digital predistortion of RF power amplifier," *IEEE Access*, vol. 7, pp. 59832–59843, 2019.

[9] M. Rawat, P. Roblin, C. Quindroit, K. Salam, and C. Xie, "Digitally supported feed-forward harmonic cancellation for filter-less ultra-wideband transmitters," in *Proc. IEEE Int. Microw. RF Conf. (IMaRC)*, Bengaluru, India, Dec. 2014, pp. 84–87.

[10] H. Yu, V. Ratnasamy, P. Roblin, M. Rawat, and C. Xie, "Automatic feed-forward cancellation of modulated harmonic," in *Proc. 86th ARFTG Microw. Meas. Conf.*, Atlanta, GA, USA, Dec. 2015, pp. 1–3.

[11] M. Rawat, P. Roblin, C. Quindroit, N. Naraharisetti, R. Pond, K. Salam, and C. Xie, "Characterization and modeling scheme for harmonics at power amplifier output," in *Proc. 83rd ARFTG Microw. Meas. Conf.*, Tampa, FL, USA, Jun. 2014, pp. 1–4.

[12] M. Rawat, P. Roblin, C. Quindroit, K. Salam, and C. Xie, "Concurrent dual-band modeling and digital predistortion in the presence of unfilterable harmonic signal interference," *IEEE Trans. Microw. Theory Techn.*, vol. 63, no. 2, pp. 625–637, Feb. 2015.

[13] C. Li, Y. Yamao, and S. He, "Multi-cell harmonics and intermodulation compensation architecture for concurrent dual-band transmitters," in *Proc. IEEE Topical Conf. RF/Microwave Power Model. for Radio Wireless Appl. (PAWR)*, Phoenix, AZ, Jan. 2017, pp. 63–65.

[14] P. Jaraut, M. Rawat, and F. M. Ghannouchi, "2D curtailed harmonic memory polynomial for reduced complexity in concurrent dual-band modelling and digital predistortion with the second band at harmonic frequency," *IET Commun.*, vol. 12, no. 12, pp. 1438–1447, Jul. 2018.

[15] P. Jaraut, M. Rawat, and F. M. Ghannouchi, "Harmonically related concurrent tri-band behavioral modeling and digital predistortion," *IEEE Trans. Circuits Syst. II, Exp. Briefs*, vol. 66, no. 6, pp. 1073–1077, Jun. 2019.

[16] Datasheet CREE Inc. *CGH40010 10W GaN HEMT*. Accessed: Nov. 2019. [Online]. Available: https://www.cree.com

[17] *Datasheet AD-FMCOMMS5-EBZ, and AD9361: RF Agile Transceiver*. Accessed: Nov. 2019. [Online]. Available: https://www.analog.com/en/design-center/evaluation-hardware-and-software/evaluation-boards-kits/eval-ad-fmcomms5-ebz.html#eb-overview

[18] G. C. Tripathi and M. Rawat, "Delay compensation for 4G/5G transmitter system characterization," *Microw. Opt. Technol. Lett.*, vol. 59, no. 8, pp. 1887–1890, Aug. 2017.

[19] M. Rawat and F. M. Ghannouchi, "A mutual distortion and impairment compensator for wideband direct-conversion transmitters using neural networks," *IEEE Trans. Broadcast.*, vol. 58, no. 2, pp. 168–177, Jun. 2012.

[20] C. Pathak and K. Rawat, "Nonlinear characterization and distortion mitigation in six-port modulator," *IEEE Trans. Instrum. Meas.*, vol. 68, no. 4, pp. 1178–1188, Apr. 2019.

[21] M. T. Hagan and M. B. Menhaj, "Training feedforward networks with the Marquardt algorithm," *IEEE Trans. Neural Netw.*, vol. 5, no. 6, pp. 989–993, Nov. 1994.

[22] M. Rawat and F. M. Ghannouchi, "Distributed spatiotemporal neural network for nonlinear dynamic transmitter modeling and adaptive digital predistortion," *IEEE Trans. Instrum. Meas.*, vol. 61, no. 3, pp. 595–608, Mar. 2012.

[23] D. Huang, H. Leung, and X. Huang, "Experimental evaluation of predistortion techniques for high-power amplifier," *IEEE Trans. Instrum. Meas.*, vol. 55, no. 6, pp. 2155–2164, Dec. 2006.

[24] M. T. Hagan and M. B. Menhaj, "Training feedforward networks with the marquardt algorithm," *IEEE Trans. Neural Netw.*, vol. 5, no. 6, pp. 989–993, Nov. 1994.

[25] M. Rawat and F. M. Ghannouchi, "Distributed spatiotemporal neural network for nonlinear dynamic transmitter modeling and adaptive digital predistortion," *IEEE Trans. Instrum. Meas.*, vol. 61, no. 3, pp. 595–608, Mar. 2012.

[26] D. Huang, H. Leung, and X. Huang, "Experimental evaluation of predistortion techniques for high-power amplifier," *IEEE Trans. Instrum. Meas.*, vol. 55, no. 6, pp. 2155–2164, Dec. 2006.

[27] Datasheet of Switched Harmonic Filter Bank. *SFB026*. Accessed: Nov. 2019. [Online]. Available: https://www.sarastech.co.uk/wp-content/uploads/2019/07/SFB026-6CH-SWFB-Data-Sheet-Rev1.pdf

[28] H.-M. Tsai, P.-J. Chou, and C.-Y. Chang, "A novel filter bank using serial-switched structure," in *Proc. Asia–Pacific Microw. Conf. (APMC)*, New Delhi, India, Dec. 2016, pp. 1–3.

[29] K. Entesari, K. Obeidat, A. R. Brown, and G. M. Rebeiz, "A 25–75-MHz RF MEMS tunable filter," *IEEE Trans. Microw. Theory Techn.*, vol. 55, no. 11, pp. 2399–2405, Nov. 2007.

[30] *Datasheet 310-020050-XXX Configurable Switched Filter Banks*. Accessed: Nov. 2019. [Online]. Available: http://micro.apitech.com/pdf/sfb/310-020050-xxx-configurable-switched-filter-banks.pdf

[31] P. Jaraut, M. Rawat, and F. M. Ghannouchi, "Composite neural network digital predistortion model for joint mitigation of crosstalk, i/q imbalance, nonlinearity in MIMO Transmitters," *IEEE Trans. Microw. Theory Techn.*, vol. 66, no. 11, pp. 5011–5020, Nov. 2018.

[32] G. Keren, N. Cummins, and B. Schuller, "Calibrated prediction intervals for neural network regressors," *IEEE Access*, vol. 6, pp. 54033–54041, 2018.

[33] H. Kabir, L. Zhang, M. Yu, P. Aaen, J. Wood, and Q.-J. Zhang, "Smart modeling of microwave devices," *IEEE Microw. Mag.*, vol. 11, no. 3, pp. 105–118, May 2010.

[34] *Datasheet ZC706 Evaluation Board*. Accessed: Nov. 2019. [Online]. Available: https://www.xilinx.com/support/documentation/boards_and_kits/zc706/ug954-zc706-eval-board-xc7z045-ap-soc.pdf

HEMANT KUMAR SINGHAL (Member, IEEE) received the B.Tech. degree in electronics and communication engineering from the Government College of Engineering Ajmer, Rajasthan Technical University, Kota, and the Master of Technology degree in radio frequency design and technology from IIT Delhi, in 2014. He is currently pursuing the Ph.D. degree with the Indian Institute of Technology (IIT) Roorkee. He was a Lecturer with the Rajiv Gandhi University of Knowledge Technologies (RGUKT), Basar, from 2014 to 2015. He is an Assistant Professor with the Department of Electronics and Communication, National Institute of Technology (NIT), Uttarakhand, India. His current research interests include radio frequency power amplifier, transceiver design, and radio frequency active and passive circuits design.

KARUN RAWAT (Senior Member, IEEE) received the Ph.D. degree in electrical engineering from the University of Calgary, Calgary, AB, Canada, in 2012. He was a Scientist with the Space Applications Center, Indian Space Research Organization, Ahmedabad, India, from 2003 to 2007. He was an Assistant Professor with the Centre for Applied Research in Electronics, IIT Delhi, New Delhi, India, from 2013 to 2014. He was also a Student Research Assistant, a Postdoctoral Research Fellow under the research grant of iCORE, and the CRC Chair with the University of Calgary. He is currently an Associate Professor with the Department of Electronics and Communication Engineering, IIT Roorkee, Roorkee, India. His research involvement has resulted in over 67 publications in journals and conferences, two published books, and one book chapter. He holds over two patents. His current research interests include microwave active and passive circuit design and advanced transmitter and receiver architecture for software-defined radio applications.

Dr. Rawat is a member of the IEEE MTT 12 Microwave High power Techniques Committee. He received the Research Production Award from the University of Calgary for three consecutive years, from 2009 to 2012. Under his leadership, the University of Calgary Team received First Prize and the Best Design Award with the Third Annual Smart Radio Challenge, in 2010, through the Wireless Innovation Forum, while competing against five universities from the U.S. and Japan. He is a Reviewer of the several IEEE TRANSACTIONS.

• • •